Open access • Journal Article • DOI:10.1103/PHYSREVB.61.12233

Mn-55 NMR and NQR study of the cubic Laves-phase compound UMn2

Saurav Giri, Hiroyuki Nakamura, Masayuki Shiga

Institutions: Kyoto University

Published on: 01 May 2000 - Physical Review B (AMERICAN PHYSICAL SOC)

Topics: Nuclear quadrupole resonance, Knight shift, Relaxation (NMR), Electric field gradient and Laves phase

Mn-55 NMR and NQR study of the cubic Laves-phase compound UMn2

AUTHOR(S):

Giri, S; Nakamura, H; Shiga, M

PHYSICAL REVIEW B VOLUME 61, NUMBER 18 1 MAY 2000-II

^{55}Mn NMR and NQR study of the cubic Laves-phase compound UMn_2

Saurav Giri, Hiroyuki Nakamura, and Masayuki Shiga
Department of Materials Science and Engineering, Kyoto University, Kyoto 606-8501, Japan
(Received 25 October 1999)

We performed ^{55}Mn NMR and nuclear quadrupole resonance (NQR) measurements of a cubic Laves-phase compound UMn_2, which shows structural instability in the temperature range 210–240 K. NMR and NQR signals of two different crystallographic Mn sites, which are in nearly axial and nonaxial electric field gradients, were found below structural transitions, being consistent with the crystal structure determined from diffraction analysis and confirming the absence of magnetic ordering. Analysis of the Knight shift shows that the spin component of the isotropic hyperfine coupling constant does not change at the phase transitions, and the anisotropy of the Knight shift appreciably depends on temperature. The nuclear spin-lattice relaxation is not enhanced except around the structural transitions and is explained as simple conduction-electron relaxation, indicating absence of localized moments at both U and Mn sites. The relaxation behavior also suggests neither critical behavior nor strong electron correlation in the low-temperature range.

I. INTRODUCTION

The subject of moment stability and magnetic order in the presence of topological frustration in the Laves-phase compounds RMn_2 (R = rare earth) continues to attract a great deal of experimental and theoretical attention. The stability of manganese moment is closely related to the lattice parameter, i.e., the Mn-Mn distance.[1–3] In general magnetic moment in the Mn sublattice becomes unstable when the Mn-Mn distance is below a critical value ($\simeq$2.7 Å), resulting in nonmagnetic Mn atoms. On the other hand, the compounds have stable moment when the lattice parameter is above the critical value. Magnetic structures in magnetically ordered states are complicated because of competing interactions among R-R, Mn-Mn and R-Mn. In the vicinity of the critical lattice parameter, a mixed phase, in which magnetic and nonmagnetic Mn atoms coexist, was observed by microscopic probes such as neutron diffraction, nuclear magnetic resonance (NMR), and Mössbauer experiments.[4–9] Due to the Mn moment instability, Mn atoms in RMn_2 can be magnetic or nonmagnetic depending on the rare earth element, temperature, pressure, etc.

On the other hand, uranium magnetism has also been investigated extensively. The $5f$ electrons may be itinerant or localized depending on the local environment. The interplay between the two state gives rise to exotic phenomena like heavy-fermion and spin-fluctuation behaviors. The stability of U localized moment is related with the U-U interatomic distance. It has been argued that U compounds have localized moments when the U-U distance is larger than the critical value ($\simeq$3.5 Å), so-called Hill limit.[10] The Laves-phase compounds UT_2 (T = transition metal) are attractive candidates to study the U moment instability since the U-U distance in UT_2 distributes around the critical value depending on T.

The Laves-phase compound UMn_2 exhibits the $C15$ cubic structure (space group $Fd\bar{3}m$) with the lattice parameter a = 7.16 Å at room temperature.[11,12] UMn_2 undergoes a rhombohedral distortion to the space group $R\bar{3}m$ on cooling below ~240 K. Further cooling below below ~210 K results in a second structural change to the orthorhombic space group *Imma*.[12–15] These transition temperatures seem to slightly depend on samples (about ±10K). Despite the discontinuity of lattice constants at the transitions, the variation in unit cell volume is continuous with temperature.[14]

Although the susceptibility shows a Curie-Weiss-like behavior with an effective moment 4.15 μ_B at high temperatures (>420 K),[16] the temperature dependence of the susceptibility (see the inset in Fig. 6) is weak at the lower temperatures and shows a maximum at ~240 K,[17,18] which was speculated to be an antiferromagnetic transition temperature at an early stage of the study.[17] The specific heat shows a λ-type anomaly at ~240 K,[15] suggesting a second-order transition. On the other hand, no evidence of magnetic ordering has been found in neutron diffraction studies.[11] A Mössbauer study on $U(Mn_{0.9}Fe_{0.1})_2$ also exhibits the absence of localized moment.[19] Therefore, the ground-state magnetic properties of UMn_2 have attracted much interest. The susceptibility shows a marked upturn below ~50 K, although there seems to be a strong sample dependence.[16–18] Like isomorphous UAl_2, which is one of strongly correlated U compounds, UMn_2 exhibits a T^2 dependent resistivity at low temperatures,[18] together with an enhanced γ of 41 mJ/mol K^2 in specific heat,[15] suggesting strong spin fluctuations. The muon spin relaxation rate discontinuously changes below ~40 K,[15], where the susceptibility shows a marked upturn on further cooling, suggesting possible U spin fluctuations.

As another aspect of UMn_2, the structural instability of the cubic Laves phase has attracted much attention. It is now a general consensus that the structural transition is not accompanied by magnetic ordering. Among a number of Laves phases only a few of them exhibit such a low-temperature structural instability. However, the physical mechanism for the lattice instability remains to be explained.

Thus UMn_2 locates an interesting position in the study of manganese and uranium magnetism. However, the nature of the magnetic state of UMn_2 remains controversial and needs

further investigations. Nuclear magnetic and quadrupole resonances (NMR and NQR) are useful microscopic methods to study microscopic magnetic properties. To the best of our knowledge there has been no NMR/NQR work of UMn_2. In the present study, we report the results of ^{55}Mn NMR and NQR experiments on UMn_2.

II. EXPERIMENTAL PROCEDURES

A polycrystalline ingot of UMn_2 was prepared by using a tri-arc furnace in an argon atmosphere at the Oarai Branch, Institute of Materials Research, Tohoku University. For nuclear resonance experiments the ingot was crushed into fine powder in an inert atmosphere. To insulate each particle the powder was soaked in paraffin.

NMR and NQR measurements were carried out with a phase-coherent pulsed spectrometer. The nuclear spin-lattice relaxation time, T_1, was measured by observing the recovery of the NQR or NMR spin-echo after the saturation of nuclear spin levels by a single RF pulse. The nuclear gyromagnetic ratio for ^{55}Mn, $^{55}\gamma/2\pi = 1.050$ MHz/kOe, was used for analysis.

Details of the structural data for UMn_2 are summarized: Above 240 K the structure is of the cubic $C15$ type, whose space group is $Fd\bar{3}m$. Uranium and manganese atoms occupy the $8a$ site with $\bar{4}3m$ local symmetry and the $16d$ site with $\bar{3}m$ local symmetry, respectively. The $16d$ site is described as a network of corner-sharing regular tetrahedra, which is one of the typical geometrically frustrated lattices. A ^{55}Mn nucleus (nuclear spin $I=\frac{5}{2}$) at the $16d$ site feels a finite electric field gradient (EFG), $eq=V_{zz}$, with the zero asymmetry parameter, $\eta=(V_{xx}-V_{yy})/V_{zz}$, where V_{xx}, V_{yy}, and V_{zz} are diagonal components of the EFG tensor. According to Lawson *et al.*,[13,14] UMn_2 undergoes a rhombohedral structural distortion to the space group $R\bar{3}m$ at $\sim$240 K. Further decreasing temperature it exhibits a second structural transition at $\sim$210 K to an orthorhombic crystal structure with the space group $Imma$. The orthorhombic phase is obtained by the shearing of a pair of counter (100) planes of the cubic phase. The orthorhombic lattice constants, a_o, b_o and c_o are equal to $a_c/\sqrt{2}$, $a_c/\sqrt{2}$ and a_c, respectively, in the limit of no distortion, where a_c means the lattice constant of the cubic phase. Lawson *et al.*[14] reported $a_o=4.8163$ Å, $b_o=5.2478$ Å and $c_o=7.1820$ Å at 12 K. Then, the distortion to the a_o and b_o directions are approximately 4–5 % at 12 K. In the orthorhombic phase, U atoms occupy the $4e$ site with $mm2$ local symmetry and the manganese site separates to two different sites, i.e., $4b$ and $4d$ sites. The relation between the $16d$ Mn site in the cubic phase and the $4b$/$4d$ sites is sketched in Fig. 1. Associated with the orthorhombic distortion, two of four Mn atoms in a tetrahedron approach each other and the other two become more distant. As a result, the Mn site separates to two different crystallographic sites with the same population ratio. The axial symmetry is lost in the $4b$ and $4d$ sites; site symmetry of both the sites is $2/m$. Therefore, we expect EFG with finite η for both the sites. However, symmetry considerations taking into account only point charge on nearest neighbor atomic sites indicates larger η for the $4d$ site than the $4b$ site. The local principal axis at both the sites is expected to lie in the c plane.

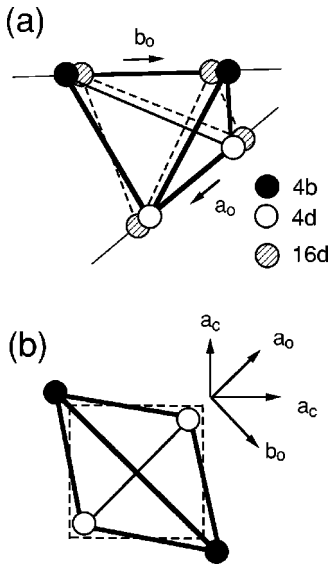

FIG. 1. Mn sites in UMn_2. One tetrahedron formed by four Mn atoms is shown. Figure (a) shows the distortions of atomic displacement in the orthorhombic phase with respect to the cubic phase. Figure (b) shows a projection on the c plane of the orthorhombic structure, where the distortion is exaggerated. Closed and open circles represent nearly axial $4b$ and nonaxial $4d$ sites, respectively.

III. EXPERIMENTAL RESULTS

A. NQR results

At 4.2 K and in the zero external field condition, we found several nuclear resonance lines, which are shown in Fig. 2. Two pairs of lines were found at around 4 and 8 MHz. All the lines are well reproduced by Lorentzian functions as shown by solid curves in the figure. These lines are interpreted as ^{55}Mn NQR. For the nuclear spin $I=\frac{5}{2}$ and in the case of sufficiently small η, the NQR lines are, in general, observed at

$$\nu_1=\nu_Q\left(1+\frac{59}{54}\eta^2\right), \quad \nu_2=2\nu_Q\left(1+\frac{11}{54}\eta^2\right), \qquad (3.1)$$

where

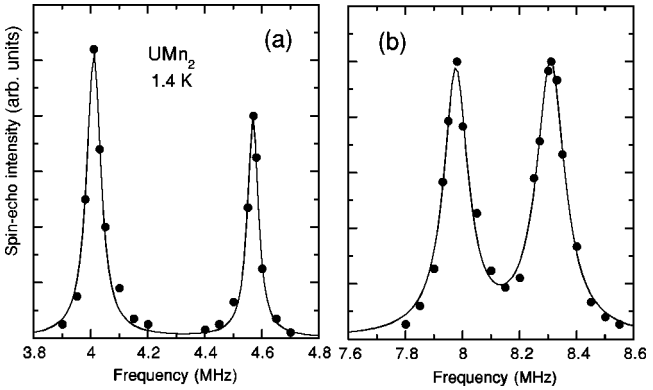

FIG. 2. ^{55}Mn NQR lines at 1.4 K. The resonances in (a) and (b) correspond to the transitions of $m=\pm1/2\leftrightarrow\pm3/2$ and $m=\pm3/2\leftrightarrow\pm5/2$, respectively.

$$\nu_Q = \frac{3e^2qQ}{2hI(2I-1)} \tag{3.2}$$

is the quadrupole resonance frequency. The low- and high-frequency lines, ν_1 and ν_2, correspond to transitions of $m = \pm\frac{3}{2} \leftrightarrow \pm\frac{1}{2}$ and $m = \pm\frac{5}{2} \leftrightarrow \pm\frac{3}{2}$, respectively. The experimental result indicates that at low temperature there are two different Mn sites which feel different EFG. The lines centered at $\nu_1 = 4.010 \pm 0.001$ and $\nu_2 = 7.977 \pm 0.002$ MHz are assigned to one of the sites and those at $\nu_1 = 4.569 \pm 0.001$ and $\nu_2 = 8.309 \pm 0.002$ MHz to the other. On using Eq. (3.1), we obtain two sets of quadrupolar parameters $\nu_Q = 3.992 \pm 0.001$ MHz and $\eta = 0.065 \pm 0.003$, and $\nu_Q = 4.219 \pm 0.001$ MHz and $\eta = 0.282 \pm 0.001$, from the former and latter sets of the lines, respectively. We also confirmed by the numerical diagonalization of the full nuclear spin Hamiltonian that Eq. (3.1) is valid for these η values. These η values indicate that one of the Mn sites feels roughly axial EFG whereas the other feels more asymmetric EFG. Hereafter, we will call them *axial* and *nonaxial* sites, which are considered to correspond to the $4b$ and $4d$ Mn sites, respectively, in the orthorhombic phase taking account of the symmetry consideration given in last section. The spectral intensity seems to be consistent with the 1:1 population ratio of the $4b$ and $4d$ sites. Thus the present NQR results are in good agreement with the crystallographic results. At the same time, the observation of NQR confirms no magnetic ordering at least down to 1.4 K, being in accordance with the results of other microscopic experiments.[11,19,15]

The temperature variation of the NQR frequencies ν_2 were followed up to 200 K for both the sites and plotted in Fig. 3. Intensities are too poor to be detected above 200 K. Instead, crude values of $\sim 2\nu_Q$ estimated from first-order satellite edges of the NMR spectrum (will be discussed in next subsection) arising from the *axial* site ($16d$ site of the cubic $C15$ phase above 240 K) are also plotted in the figure. Above the structural transition at $\sim$240 K, the resonance frequency shows weak temperature dependence, while below $\sim$240 K the frequency separates to two different components, which start to decrease with decreasing temperature. At the rhombohedral-orthorhombic transition ($\sim$210 K), no appreciable anomaly was found. Generally the origin of EFG consists of two contributions; one is of intra-atomic electron configurations and the other is the lattice and conduction-electron term made up of outside charge. The reduction of ν_Q below 240 K may be related to the symmetry lowering of the crystal and/or electron configurations. It is notable that the temperature variation of ν_Q (and probably also η) is continuous at the transition points.

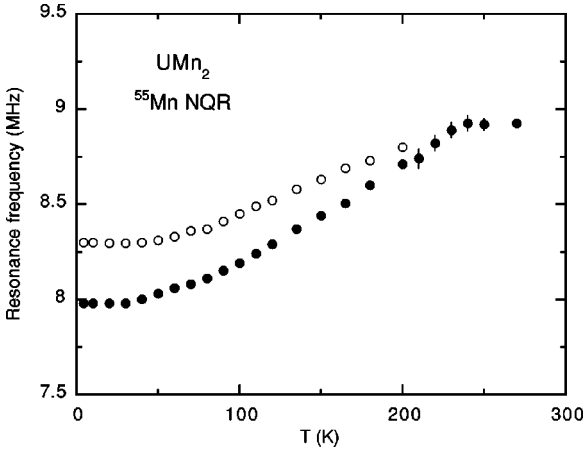

FIG. 3. Temperature variations of the NQR frequency corresponding to transitions of $m = \pm 5/2 \leftrightarrow \pm 3/2$. The closed and open circles represent the *axial* and *nonaxial* sites, respectively. The data above 200 K were estimated from first-order satellites of field-swept spectra.

B. NMR results

We measured field-swept spectra in the high-field condition to check the quadrupolar parameters and to estimate the values of the Knight shift. Here, we determine the parameters by mainly comparing experimental spectra with computer simulated line shapes. Assuming the coincidence of the principal axes of the Knight shift and EFG tensors, and within the second-order perturbation limit of the quadrupolar interaction, the resonance frequency of the $m \leftrightarrow m-1$ transitions as a function of the angles between the external field and EFG axes, θ and ϕ, is given by[20,21]

$$\begin{aligned}\nu_m(\theta,\phi) = {} & \nu_0(1+K_{\rm iso}) + \tfrac{1}{2}\nu_0 K_1(3\cos^2\theta - 1) - \tfrac{1}{2}\nu_0 K_2 \sin^2\theta\cos 2\phi + \tfrac{1}{2}\nu_Q(m-\tfrac{1}{2})(3\cos^2\theta - 1 - \eta\sin^2\theta\cos 2\phi) \\ & + \frac{\nu_Q^2}{32\nu_0}\sin^2\theta(g_C\cos^2\theta - g_B) + \frac{\eta\nu_Q^2}{48\nu_0}\sin^2\theta(g_C\cos^2\theta + g_B)\cos 2\phi \\ & + \frac{\eta^2\nu_Q^2}{72\nu_0}\{g_A - (g_A+g_B)\cos^2\theta - \tfrac{1}{4}g_C\sin^4\theta\cos^2 2\phi\},\end{aligned} \tag{3.3}$$

with

$$\begin{aligned} g_A &= 24m(m-1) + 9 - 4I(I+1), \\ g_B &= 6m(m-1) + 3 - 2I(I+1), \\ g_C &= 4g_A + g_B, \end{aligned}$$

and with a conventional definition for the Knight shift,

$$\begin{aligned} K_{\rm iso} &= \tfrac{1}{3}(K_X + K_Y + K_Z), \\ K_1 &= \tfrac{1}{3}(2K_Z - K_X - K_Y), \\ K_2 &= K_Y - K_X, \end{aligned} \tag{3.4}$$

where K_X, K_Y and K_Z are diagonal components of the Knight shift tensor. The resonance field $[H_m(\theta,\phi)]$ of the constant-frequency experiment is obtained by solving Eq. (3.3) for $H_m(\theta,\phi) = \nu_0/\gamma$ where ν_m is the operating frequency. The coincidence of the principal axes of the Knight shift and EFG tensors is not necessarily justified in the low-symmetric phases, but it was found that this assumption does not lead to serious contradiction to the analysis of UMn_2. In the case of a homogeneous distribution of the powder orientation, the theoretical field-swept powder pattern for the $m \leftrightarrow m-1$ transitions is calculated as

$$S_m(H) = \left\{ \frac{d^2 H_m(\theta,\phi)}{\sin\theta \, d\theta \, d\phi} \right\}^{-1}. \tag{3.5}$$

The actual spectrum is obtained by convoluting an appropriate distribution function, $g(\nu)$, as

$$I_m(H) = C \int g(H-H') S_m(H) dH'. \tag{3.6}$$

where C is a normalizing constant. The whole line shape is given by summing up all m components. The computer generated line shape thus obtained is compared with experimental spectra.

Examples of field-swept ^{55}Mn NMR spectra of UMn_2 measured at 76.3 MHz are shown in Fig. 4(a), all of which locate at around the zero Knight shift position. Above 240 K the NMR spectrum consists of a single component with sharp first-order quadrupolar satellites, being consistent with a unique Mn site with $\eta = 0$. The center line, i.e., the transitions of $m = -\frac{1}{2} \leftrightarrow m = +\frac{1}{2}$, shows a double peak structure, which is a typical second-order quadrupolar powder pattern. On the other hand, at low temperatures we observed smeared satellite and center-line structures. Nevertheless the line shape can satisfactorily be explained assuming the presence of two different chemical sites. Figure 4(b) shows calculated lines using the quadrupolar parameters obtained from the NQR analysis for the *axial* and *nonaxial* sites at 4.2 K, where we used appropriate values of the Knight shift (discussed below). The first-order satellites of both the sites are rounded out to certain extents due to the appearance of η. The total spectrum is thus obtained as a sum of two components, which is also shown in Fig. 4(b) after convoluting a Gaussian function with an appropriate width. The calculated line shape reproduces satisfactorily the experimental spectrum at 4.2 K. In the intermediate temperature range of 210–240 K the situation seems to be more complicated, which will be discussed by simulating the center-line shape.

Examples of only center lines measured at different temperatures are shown in Fig. 5(a). Above 240 K, the line shape can again be reproduced with a single component with appropriate quadrupolar and Knight shift parameters; see the result at 250 K in Fig. 5(a), where bold and fine solid curves indicate calculated $S_{1/2}(H)$ and $I_{1/2}(H)$, respectively. Note that the spectral shape, especially the separation between two peaks, cannot be reproduced without introducing nonzero K_1 indicating an appreciable anisotropy of the Knight shift. Below 210 K center lines are well reproduced by assuming two components with appropriate quadrupolar and Knight shift values; see the spectrum at 160 K in Fig. 5(a). Figure 5(b)

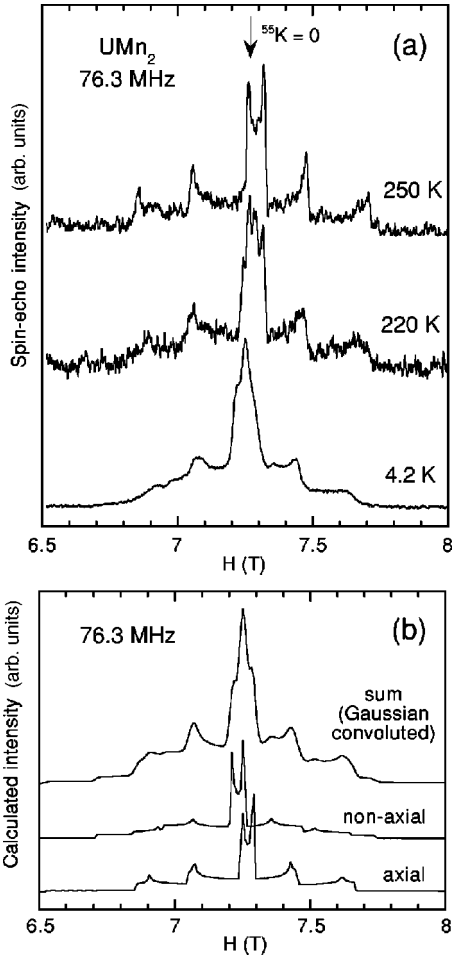

FIG. 4. (a) Examples of field-swept NMR full spectra measured at 76.3 MHz. (b) Calculated powder patterns with quadrupolar parameters estimated from NQR experiments at 4.2 K and appropriates values of the Knight shift.

shows the temperature dependence of the center line spectrum measured in the intermediate temperature range around the phase transitions. Below 240 K, additional components appear other than the *axial* component. The new components seem to exhibit a broad inhomogeneous linewidth. Neutron diffraction experiments by Lawson *et al.*[14] suggested the coexistence of the $R\bar{3}m$ and *Imma* phases in the temperature range, which gives rise to more than two or a distribution of chemical sites. Therefore, our NMR results seem to be consistent with the diffraction analysis. Here, tentatively, we try to simulate the line shape assuming the presence of only two different components as below 210 K. As shown in Fig. 5(a) (the spectrum at 220 K), the line shape can roughly be reproduced. The obtained quadrupolar and Knight-shift parameters show a reasonably continuous temperature variation (see Figs. 3 and 6).

To evaluate the Knight shift we assume uniaxial anisotropy ($K_2 = 0$) of the principal shift tensors for all the temperature range. This is reasonable above 240 K, where the Mn site is axially symmetric, while below 240 K it is just an assumption for simplicity. Figure 6 shows the temperature dependence of the Knight shift obtained by analyzing the whole spectra (including both center and satellite lines) mea-

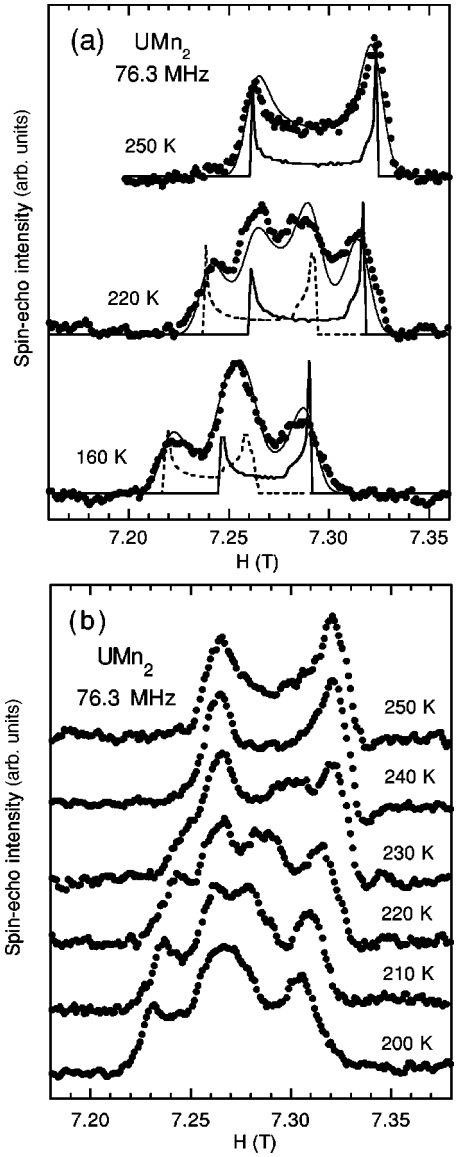

FIG. 5. (a) Examples of field-swept NMR center-line spectra measured at 76.3 MHz. The bold solid and broken curves represent calculated powder patterns for the *axial* and *nonaxial* sites, respectively. Fine solid curves indicate total spectra after the convolution of Gaussian functions with appropriate widths. Figure (b) shows evolutions of center-line spectra around the structural transitions.

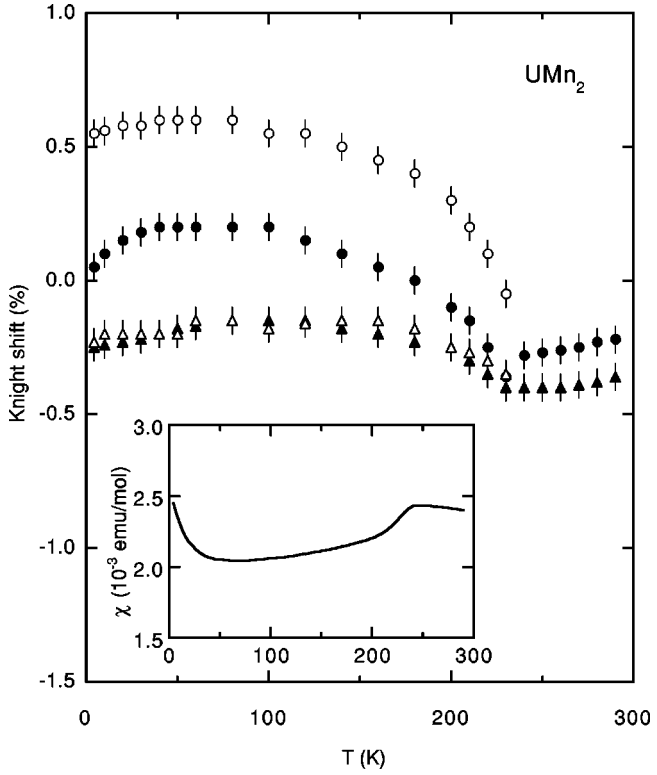

FIG. 6. Temperature dependences of isotropic (K_{iso}, circles) and anisotropic (K_1, triangles) components of the Knight shift for the *axial* (filled marks) and *nonaxial* (open marks) sites. The inset shows the temperature dependence of the susceptibility.

sured at several different frequencies. These values may include some ambiguity below 240 K due to the simplification of $K_2=0$ but are enough reliable above 240 K. The anisotropic components K_1 (for both the *axial* and *non-axial* components) are slightly negative in all the temperature range and show rather appreciable temperature dependences. There is no site dependence of K_1 within the experimental accuracy. The isotropic components K_{iso} are negative at high temperatures and increase to positive values on further cooling from 240 K. Below the structural transition, K_{iso} depends on the site. Below $\sim$50 K, one can see slight reductions of K_{iso}. The Knight shift is discontinuous with temperature at $\sim$240 K but not at $\sim$210 K. If the temperature dependence is caused by the Mn 3*d*-spin component only, as usually in 3*d* magnets, the positive K_{iso} at low temperatures suggests a comparable or larger positive offset of Van Vleck–type orbital and/or conduction-electron contributions because the on-site *d*-spin hyperfine coupling (via core polarization) is always negative. The transferred hyperfine field from U moments, if any, may be one of the origins of the temperature dependence but is expected to be much smaller than the on-site Mn-3*d* contribution.

Figure 7 shows the isotropic component of the Knight shift plotted against the susceptibility with the temperature as an implicit parameter (K-χ plot). For this analysis, we measured the temperature dependence of the susceptibility of the present sample, which is shown in the inset of Fig. 6 and is basically the same as that reported in Ref. 18. Above 240 K, K_{iso} is in proportion to χ (the broken line). Below 240 K, the points lie on different straight lines depending on the sites (full lines). It is interesting to note that the isotropic part of the hyperfine coupling constants, A_{iso} obtained from the slopes of the lines do not change at 240 K and do not depend on the site within the experimental accuracy, indicating that the spin component of the hyperfine coupling does not change at the structural transformation. Note that the coupling constants are the same for both the *axial* and *nonaxial* sites in spite of different absolute values of K_{iso}, implying that only temperature independent terms depend on the site. We cannot find a notable discontinuity at 210 K again. The hyperfine coupling constant is estimated from the K-χ plot as $A_{iso}=2N\mu_B dK_{iso}/d\chi=-220\pm20$ kOe/μ_B (where, N and μ_B are Avogadoro's number and the Bohr magneton, respectively), on the assumption that only Mn moments contribute to the temperature dependence of susceptibility through out the whole temperature range, though the contribution of U

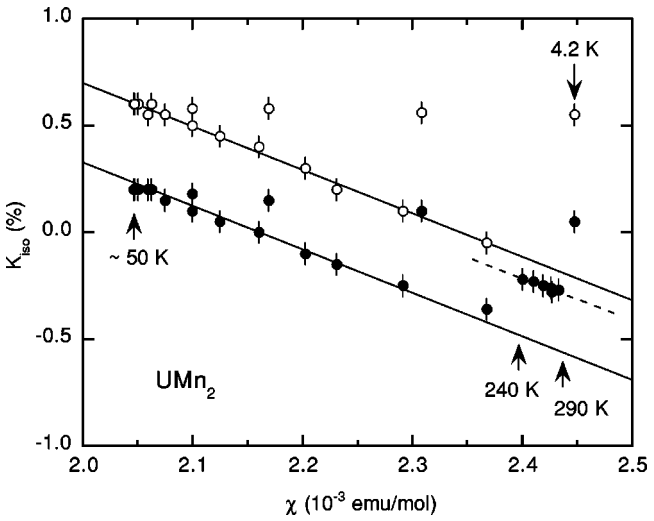

FIG. 7. The isotropic component of the Knight shift plotted against the susceptibility with temperature as an implicit parameter (K-χ plot). Closed and open circles represent the *axial* and *non-axial* sites, respectively. The broken and full straight line gives hyperfine coupling constants for the high-temperature cubic and low-temperature orthorhombic phases, respectively.

magnetism cannot be excluded. The value of A_{iso} for UMn_2 is large compared to the value of other RMn_2 systems in the ordered state.[6,22] However, this value is comparable to the value of YMn_2 in the paramagnetic state.[23,24] Below ~50 K, the plots deviate markedly from the straight lines and seem to come on other lines with different slopes. This phenomenon may be related to a marked upturn of the susceptibility on further cooling, and hence to a certain evolution of the electronic state suggested, for example, by muon spin relaxation measurements.[15] However, since it is known that the low-temperature susceptibility strongly depends on samples, we do not discuss further the low-temperature anomaly.

It should be noted that the temperature dependence of the anisotropic Knight shift K_1 is appreciable. If we formally assume that the susceptibility is isotropic, the anisotropic component A_{aniso} $[=\frac{2}{3}(A_{\parallel}-A_{\perp})]$ is roughly estimated form the K_1-χ plot to be $A_{aniso}\simeq -80$ and -140 kOe/μ_B for below and above the structural transition, respectively. These are the coupling constants particularly estimated from the *temperature-dependent* part of K_1. These magnitudes are appreciably large and comparable to the isotropic component. It is interesting to note that A_{aniso} reduces to about half at the structural transitions in contrast to no change in A_{iso}. The origin of this large anisotropy is of interest. In general, the anisotropy is caused by dipole or orbital contribution, and the Van Vleck-type orbital contribution is independent of temperature. Since the magnitude are apparently much larger than the conventional lattice dipolar field, it is presumed that the LS coupling is rather large in UMn_2 and that the effect of the nonquenched Mn-3d orbitals is more or less responsible for the large *temperature-dependent* anisotropy of the Knight shift.

C. Nuclear spin-lattice relaxation time

We measured the ^{55}Mn nuclear spin-lattice relaxation time, T_1 by using NQR and NMR signals at low- and high-temperature ranges, respectively. The NQR-T_1 was measured by using ν_2 lines (transitions of $m=\pm\frac{3}{2}\leftrightarrow m=\pm\frac{5}{2}$) for both the *axial* and *nonaxial* sites. In general, the recovery of the nuclear magnetization, $M(t)$ for the $I=\frac{5}{2}$ NQR (Refs. 25 and 26) is described by two exponential functions as

$$M(t)=M_0\left\{1-a_1\exp\left(-\frac{b_1}{T_1}t\right)-a_2\exp\left(-\frac{b_2}{T_1}t\right)\right\}, \tag{3.7}$$

where t is the time between the saturation pulse and the spin-echo first pulse, and a_1, a_2, b_1 and b_2 are constants depending on η, which are given as a function of η in Ref. 26. The value of M_0 was obtained by spin-echo experiment without the saturation pulse, and the values of a and b parameters were obtained as a function of η, of which temperature dependence was taken into account properly by using the NQR results at different temperatures. Therefore, the spin-lattice relaxation time, T_1 was the only fitting parameter in Eq. (3.7). Typical recovery curves of the nuclear magnetization for both the sites (at 20 K) are shown in Fig. 8 together with the fitting of Eq. (3.7), where we took into account the site and temperature dependence of η. We found appreciably different T_1 values depending on the chemical sites; T_1 is shorter by about 30% for the *axial* site. The estimated values of $1/T_1$ vary linearly with temperature till 100 K which are plotted in the inset of Fig. 9. Average values of $1/T_1$ for the two sites are shown by open circles in Fig. 9.

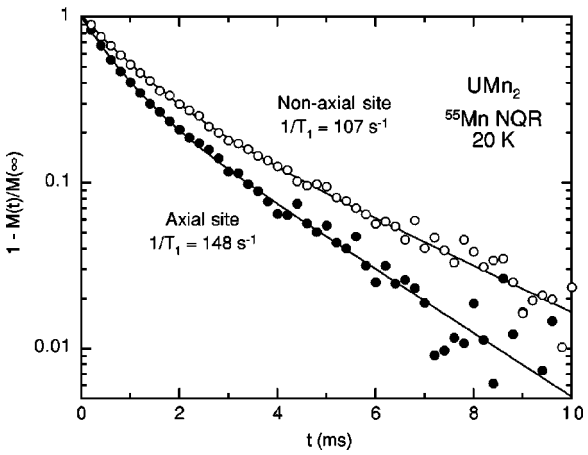

FIG. 8. Recovery of the nuclear magnetization measured by NQR for the *axial* (closed circles) and *nonaxial* (open circles) sites at 20 K. The curves indicate the fit of Eq. (3.7) with appropriate parameters.

Above ~100 K, it becomes difficult to estimate reliable T_1 values from NQR experiments due to poor signal-to-noise (S/N) ratio. Above 120 K, instead, crude values of $1/T_1$ were estimated by using superposed NMR signals in external field. The recovery of the nuclear magnetization was not described by a single exponential function. Although the distribution of chemical sites may also cause the nonsingle exponential behavior, we try to estimate rather forcibly a unique value of T_1 by attributing the behavior to the quadrupole interaction. In general, the recovery curve of the $I=\frac{5}{2}$ NMR affected by the quadrupole interaction is described by three-exponential functions as[27]

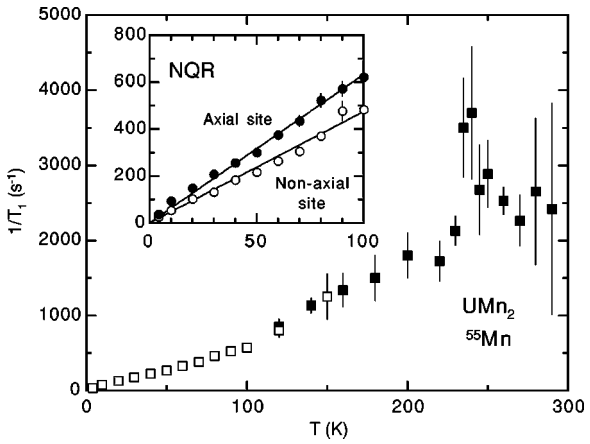

FIG. 9. The inset shows the temperature variation of the spin-lattice relaxation rate, $1/T_1$, estimated from NQR for the *axial* (closed circles) and *nonaxial* (open circles) sites, which show the $T_1T=$const behavior (straight lines). Open squares are averaged values of both the sites, and close squares represent the values estimated by NMR experiments.

$$M(t)=M_0\left\{1-c_1\exp\left(-\frac{t}{T_1}\right)-c_2\exp\left(-\frac{6}{T_1}t\right)-c_3\exp\left(-\frac{15}{T_1}t\right)\right\}. \tag{3.8}$$

The coefficients, c_1, c_2 and c_3 depend on the initial occupation condition at each nuclear level. The experimental recovery is reasonably reproduced by Eq. (3.8) with treating T_1, c_1, c_2 and c_3 as free parameters. In this analysis, due to the many fitting parameters poor S/N ratio at high temperatures results in the large ambiguity in the T_1 value. The estimated $1/T_1$ values are shown by filled squares in Fig. 9. The relaxation rate shows an anomaly at $\sim$240 K being in accordance with the structural phase transition. On the other hand, no appreciable anomaly was found at $\sim$210 K.

As seen above, $1/T_1$ is roughly linear to temperature ($T_1T=$const) at low temperatures. The constant values of $1/(T_1T)$ are 6.4 and 5.0 $s^{-1}K^{-1}$ for the *axial* and *nonaxial* sites, respectively. These values are small comparing with other *magnetic* materials. Since it is difficult to extract the contribution of conduction electron to the Knight shift from the total temperature independent Knight shift, using the above values of K_{iso}, we roughly estimate T_1TK^2 to be of the order of $10^{-6}-10^{-5}$ s K for UMn_2. In the case of Fermi gas of noninteracting spins we have $T_1TK^2=\hbar/(4\pi k_B)\times(\gamma_e/\gamma_n)^2\simeq 2\times10^{-6}$ s K (for ^{55}Mn), which is comparable to the experimental values. Thus, the relaxation is considered to be dominated by the conduction electron contribution (the Korringa mechanism), indicating clearly the absence of localized moments at both Mn and U sites and also the absence of the enhanced density of states at the Fermi level. The relaxation rates of UMn_2 are compared with another nonmagnetic RMn_2, $ScMn_2$, for which $1/(T_1T)=17.5$ $s^{-1}K^{-1}$,[28] also indicating that the electronic state of UMn_2 is less enhanced. The $T_1T=$const behavior at low temperatures indicates that there is no sign of a critical phenomena on further cooling at least down to 4.2 K, being in contrast to the susceptibility behavior. Well above the transitions, values of $1/T_1$ come on a extrapolated line from low temperatures (Fig. 9), indicating no localized magnetic moment above the transitions.

IV. DISCUSSIONS

The observation of ^{55}Mn NQR signals at low temperatures confirm microscopically that there is no magnetic ordering in UMn_2 at least down to 1.4 K, being consistent with neutron,[11] Mössbauer,[19] and μ-SR (Ref. 15) results. The two chemical Mn sites confirmed by NQR measurements below the structural transition are completely in agreement with the structural analysis by neutron diffraction.[12–14] The relaxation rate is small in all the temperature range of measurements and is explained as the Korringa-type conduction-electron relaxation, indicating that there is no localized moment on both Mn and U sites both above and below the structural transition. These experimental observations are consistent with the fact that both the Mn-Mn and U-U interatomic distances in UMn_2 ($\simeq$2.5 and $\simeq$3.4 Å, respectively) are well below the critical values ($\simeq$2.7 and $\simeq$3.5 Å, respectively) which discriminate the stability of the localized moment.

Although neither magnetic ordering nor critical behavior has been detected at the lowest temperature range, the Knight shift shows a somewhat anomalous temperature dependence below $\sim$50 K, which may be related to the marked upturn of the susceptibility[17,18] and hence to some magnetic instability at much lower temperatures.

According to high resolution diffraction experiments, UMn_2 undergoes a rhombohedral distortion to the space group $R\bar{3}m$ at $\sim$240 K and again to orthorhombic *Imma* at $\sim$210 K.[14,15] At $\sim$240 K we observed a clear symmetry breaking by NMR/NQR experiments. On the other hand, at $\sim$210 K all of the quantities measured by NMR/NQR exhibit no anomaly. These results suggest that the first rhombohedral distortion is a precursor to the orthorhombic phase and that only the transition at $\sim$240 K is a real lattice instability associated with an additional atomic displacement on further cooling. This is consistent with the fact that specific heat shows a large anomaly at $\sim$240 K but not at $\sim$210 K.

The mechanism of the lattice instability in UMn_2 is still open question. Marpoe and Lander[11] proposed that the structural transition is caused by the formation of strong $5f$ bonds of U atoms. Although they assumed the presence of localized moment at U site above the structural transition, this is not justified in various experiments and characteristic scales of U electronic energy seems to be much smaller than the transition temperature. Lawson *et al.*[14] suggested that the structural transformation in UMn_2 is reminiscent of those in other cubic Laves phases HfV_2 and ZrV_2. For these materials, recently, Chu *et al.*[29] proposed that the structural instability is due to the large density of states at the Fermi level, $\rho(E_F)$, and Fermi surface nesting, which give rise to phonon softening. This scenario does not seem to be applicable to UMn_2 because $\rho(E_F)$ is not enhanced in this material as seen from the small relaxation rate. The large temperature-dependent anisotropy of the Knight shift suggested that the effect of unquenched Mn-$3d$ orbitals is not negligible. Then, the band Jahn-Teller distortion driven mainly by Mn-$3d$ bands may be one of possible origins of the lattice instability since we may expect orbital degeneracies in the axially symmetric Mn

site in the high-temperature cubic phase. This interpretation may be consistent with the larger Knight-shift anisotropy for the high-temperature phase. However, since Mn-3d bands should come at the Fermi level in this case, it is again unlikely that the small $\rho(E_F)$ is in accord with this model. On the other hand, quite large value of γ in specific heat at low temperature[15] is in contrast to the small relaxation rate. If only U spin fluctuations are responsible to the large γ value, and if the Mn site has no substantial coupling with the U magnetism, this contradiction may be reconciled. The origin of structural instability at low temperature still remains to be explained which may highlight such ambiguity. For further understanding, calculations of electronic structures may be helpful.

In summary, we performed ^{55}Mn NMR and NQR measurements of UMn_2, which shows lattice instability at around 210–240 K. We clearly observed by NMR and NQR that the Mn-16d site in the cubic phase separates to two different crystallographic sites in the orthorhombic phase below the structural transformation (4b and 4d sites). The nuclear resonance results indicate the absence of localized moments at both Mn and U sites and also the absence of enhanced electron correlation. The origin of the lattice instability remains to be elucidated.

ACKNOWLEDGMENTS

The authors are indebted to A. Ochiai at Tohoku University, the staff members of the Oarai Branch, Institute for Materials Research, Tohoku University, A. Oyamada and H. Takahashi at Kyoto University for collaboration in the sample preparation, to T. Yamasaki for the susceptibility measurements, and to R. Iehara for technical support. One of the authors (S.G.) wishes to thank ISGRS of Kyoto University for the financial support of his work in the University.

[1] M. Shiga, Physica B **149**, 293 (1988).
[2] M. Shiga, J. Magn. Magn. Mater. **129**, 17 (1994).
[3] R. Ballou, J. Deportes, R. Lemaire, B. Ouladdiaf, and P. Rouault, in *Proceedings of the 4th International Conference on the Physics of Magnetic Materials*, edited by W. Gorzkowski, H. K. Lachowicz, and H. Szymczak (World Scientific, Singapore, 1989), p. 427.
[4] C. Ritter, S. H. Kilcoyne, and R. Cywinski, J. Phys.: Condens. Matter **3**, 727 (1991).
[5] C. Ritter, R. Cywinski, S. H. Kilcoyne, and S. Mondal, J. Phys.: Condens. Matter **4**, 1559 (1992).
[6] K. Yoshimura, M. Shiga, and Y. Nakamura, J. Phys. Soc. Jpn. **55**, 3585 (1986).
[7] M. Moriwaki, H. Nakamura, and M. Shiga, J. Magn. Magn. Mater. **146**, L241 (1995).
[8] S. Giri, H. Nakamura, and M. Shiga, Phys. Rev. B **59**, 13943 (1999).
[9] K. Krop, J. Zukrowski, J. Przewoznik, J. Marzec, G. Wiesinger, Th. Häufler, G. Hilsher, and W. Steiner, J. Magn. Magn. Mater. **70**, 147 (1995).
[10] H. H. Hill, in *Plutonium*, edited by W. N. Miner (Met. Soc. AIME, New York, 1970), pp. 2–19.
[11] G. R. Marpoe and G. H. Lander, Solid State Commun. **26**, 599 (1978).
[12] A. C. Lawson, J. Less-Common Met. **L13-L16**, 30 (1983).
[13] A. C. Lawson, J. L. Smith, J. O. Wills, J. A. Orourke, J. Faber, and R. L. Hitterman, J. Less-Common Met. **107**, 243 (1985).
[14] A. C. Lawson, A. C. Larson, R. B. Von Dreele, A. T. Ortiz, and J. L. Smith, J. Less-Common Met. **132**, 229 (1987).
[15] R. Cywinski, S. H. Kilcoyne, T. Holubar, and G. Hilscher, Hyperfine Interact. **85**, 221 (1994).
[16] E. Burzo, E. Gratz, and P. Lucaci, Solid State Commun. **60**, 241 (1986).
[17] S. T. Lin and A. R. Kaufmann, Phys. Rev. **108**, 1171 (1957).
[18] E. Gratz and V. Sechovsky, Solid State Commun. **34**, 967 (1980).
[19] R. Grossinger, G. Hilscher, J. Kamesberger, H. Sassik, G. Wiesinger, V. Aechovsky, and J. Toul, J. Magn. Magn. Mater. **29**, 305 (1982).
[20] G. H. Stauss, J. Chem. Phys. **40**, 1988 (1964).
[21] M. Forsthuber, H. Nakamura, M. Shiga, and E. Bauer, Z. Phys. B **100**, 395 (1996).
[22] K. Yoshimura and Y. Nakamura, J. Phys. Soc. Jpn. **53**, 3611 (1984).
[23] G. Zheng, K. Nishikido, K. Ohnishi, Y. Kitaoka, K. Asayama, and R. Hauser, Phys. Rev. B **59**, 13 973 (1999).
[24] H. Nakamura, S. Suzuki, and M. Shiga (unpublished).
[25] D. E. MacLaughlin, J. D. Williamson, and J. Butterworth, Phys. Rev. B **4**, 60 (1971).
[26] J. Chepin and J. H. Ross, J. Phys.: Condens. Matter **3**, 8103 (1991).
[27] A. Narath, Phys. Rev. **162**, 320 (1967).
[28] K. Yoshimura, H. Nakamura, M. Takigawa, H. Yasuoka, M. Shiga, and Y. Nakamura, J. Magn. Magn. Mater. **70**, 142 (1987).
[29] F. Chu, D. J. Thoma, T. E. Mitchell, C. L. Lin, and M. Sob, Philos. Mag. B **77**, 121 (1998).